

Three-Dimensional Mesoporous Titanosilicates Prepared by Modified Sol–Gel Method: Ideal Gold Catalyst Supports for Enhanced Propene Epoxidation

A. K. Sinha,^{*,†,‡} S. Seelan,^{†,⊥} M. Okumura,[§] T. Akita,[†] S. Tsubota,^{||} and M. Haruta^{*,||}

Special Division of Green Life Technology, AIST Kansai, Midorigaoka 1-8-31, Ikeda 563-8577, Japan, Department of Chemistry, Graduate School of Science, Osaka University, Osaka 560-0043, Japan, and Research Institute for Green Technology, AIST, Onogawa 16-1, Tsukuba 305-8569, Japan

Received: August 3, 2004; In Final Form: December 10, 2004

Mesoporous titanosilicates with 1–12 mol % Ti content and with three-dimensional wormhole-like mesoporosity are prepared by a modified sol–gel technique. Sorption analysis shows that there is little change in the surface properties with increasing Ti concentration in the samples, implying that Ti atoms either are well-dispersed on the walls of the silica matrix or are present inside the framework with no pore blocking effect. Spectroscopic analysis shows that the Ti atoms are atomically dispersed in the silica matrix even at very high Ti concentration and there is no observable Ti aggregate (anatase) present in the samples. These titanosilicate samples after Au deposition followed by trimethylsilylation (for enhanced hydrophobicity) are highly efficient catalysts for vapor-phase propene epoxidation using O₂ and H₂. It was possible to achieve commercially desirable performance with about 7% propene conversion, >90% propene oxide selectivity, and about 40% hydrogen efficiency.

1. Introduction

Propylene oxide (PO) is an industrially important chemical for the manufacture of polyurethane, unsaturated resins, surfactants, and other products. Industrially PO is produced using two processes: Chlorohydrin process and Halcon (hydroperoxide) process.¹ The former process produces environmentally unfriendly chlorinated organic byproducts as well as calcium chloride, while the latter process produces equimolar amounts of coproducts, is complicated, and requires heavy capital investment. Extensive efforts are being made to develop an alternative process for direct gas-phase propylene epoxidation using molecular oxygen because it is a promising method of tremendous industrial significance which can replace currently used environmentally disadvantageous processes. Enichem utilized TS-1 (MFI) as a catalyst for the epoxidation of propylene in the liquid phase using hydrogen peroxide.^{2–4} However, due to the very high production cost of H₂O₂ and its handling problems, it would be highly desirable to produce H₂O₂ in situ. Toso Co. Ltd.⁵ has developed Pd/TS-1 catalyst for the in situ generation of H₂O₂ from H₂ and O₂. Hölderich and co-workers⁶ modified the catalyst developed by Toso with Pt and reported that the improved yield of PO could be ascribed to the maintenance of Pd in its +2 oxidation state.

Our research work on the catalysis by gold^{7–9} has opened a new stage for the direct epoxidation of propylene using O₂ and H₂. In a series of papers we have reported the vapor-phase epoxidation of propylene over highly dispersed nanosize Au particles supported on TiO₂, TiO₂/SiO₂,^{10–12} and titanosilicates

such as TS-1, Ti–MCM-41 and Ti–MCM-48^{13–20} and Ti-containing hydrophobic silsesquioxane.²¹ But the problems for industrial viability still exist due to low conversion of propene, rapid deactivation, and low H₂ efficiency, which have been a major hurdle in making the process commercially viable, even though PO selectivity is >90%. Three requirements for the support to overcome these barriers are (1) isolated Ti sites which are in synergism with 2–4 nm size dispersed Au nanoparticles,^{16,22–24} (2) supports with mesopores > 5 nm for effective dispersion of Au nanoparticles inside the pores,²⁵ and (3) support hydrophobicity for better propylene oxide desorption.²⁵ Based on a rough estimate for the commercialization of vapor-phase propylene epoxidation with H₂ and O₂ our research target was one-pass propylene conversion of 10%, PO selectivity of 90%, and hydrogen efficiency of 50%.

The discovery of mesoporous materials²⁶ with a tunable pore size from 20 to 100 Å opened a way to prepare mesoporous titanosilicates, in which tetrahedral Ti can be introduced into the mesopore wall during synthesis,²⁷ such as in Ti–MCM-41,²⁸ Ti–HMS,²⁹ or grafted onto the wall surface of the mesoporous host after synthesis.³⁰ These mesoporous titanosilicates exhibit high initial catalytic activities in the selective oxidations of large alkenes using alkyl hydroperoxide and hydrogen peroxide.^{31,32} Recently, it has been shown that it is possible to enhance the activity and selectivity for epoxidation reactions by introducing hydrophobicity effects using organically modified³³ or silylated³⁴ titanosilicates. MCM-41 host has a one-dimensional pore structure, so pore blockage and diffusion limitations will reduce the utilization of active sites. Additionally, the stabilization of catalytically active Ti sites during reactions is a common challenge.³⁵ The synthesis of a new class of disordered mesoporous material with uniform channel widths interconnected in a three-dimensional wormhole-like fashion³⁶ have the advantage over the ordered MCM-type materials due to easy diffusion of reactants and products and by prevention of channel blockage. Besides, it is possible to have higher thermal stability and cheap, easy, and reproducible preparation, which is an advantage over

* To whom correspondence should be addressed. E-mails: sinha-anil@mosk.tytlabs.co.jp (A.K.S.); m.haruta@aist.go.jp (M.H.).

† Special Division of Green Life Technology, AIST Kansai.

‡ Current address: Materials Division, Toyota Central R&D Labs Inc., Nagakute, Aichi 480-1192, Japan.

§ Osaka University.

|| Research Institute for Green Technology, AIST.

⊥ Current address: Advanced Manufacturing Research Institute, AIST Chubu, 2266 Anagahora, Shimo-Shidami, Moriyama-ku, Nagoya 463-8560, Aichi, Japan.

ordered MCM-type materials, making these materials better suited for industrial applications. The possibility of tailoring the porosity of these materials (between 50 and 100 Å) allows the mesopores to be easily accessible for dispersion of 20–50 Å Au nanoparticles by deposition–precipitation (DP) method unlike in the case of narrower pores (30–40 Å) of MCM type supports where the access to mesopores by Au nanoparticles is limited.

We reported these efficient epoxidation catalysts in an earlier communication.²⁵ The main objective of the present work is to present a detailed characterization of these mesoporous titanosilicate materials and the advantages of their large pore size, 3D mesoporosity, and enhanced hydrophobicity after silylation, along with a high concentration of isolated Ti sites, in direct vapor-phase epoxidation of propene to propene oxide using molecular oxygen and hydrogen.

2. Experimental Section

2.1. Synthesis. A modified sol–gel method³⁷ was used to prepare 3D mesoporous titanosilicates (named meso-Ti–Si). It is obtained by aging, drying, and calcining a homogeneous synthesis mixture, composed of titanium butoxide, tetraethyl orthosilicate (TEOS), and organic template, triethanolamine (TEA). In a specific synthesis, titanium butoxide (0.7 g, for Ti = 2 mol %) was dropwise added to stirring TEOS (20.8 g). Then TEA (29.8 g) was added dropwise to this stirring mixture followed by the dropwise addition of deionized water (19.8 g). After the solution was stirred for 1–2 h, tetraethylammonium hydroxide (14.7 g) was added dropwise. The final homogeneous mixture with a molar ratio composition of SiO₂/0.02 TiO₂/(0.1–0.3) TMAOH/(0.25–2) C₆H₁₅O₃N/11 H₂O was aged at room temperature for 24 h, dried overnight at 100 °C, and then calcined at 700 °C for 10 h in a ramp rate of 1 °C min⁻¹ in air. For comparison, the other supports Ti–MCM-41 and Ti–MCM-48 were also synthesized (Ti = 2 mol %) according to the reported procedures.¹⁶

2.2. Deposition of Au. Gold nanoparticles were deposited on the supports by a DP method^{15–22} as described earlier. In a typical catalyst preparation an aqueous solution of HAuCl₄·4H₂O, 0.08 g (4 wt % Au wrt support), in 150 mL of water was heated to 70 °C and the pH was adjusted to 6.5 using an aqueous alkali hydroxide solution. The support, weighing 1.0 g, was suspended to it, the pH was adjusted once again to the same value, and the solution was aged at the above temperature for 1 h. The suspension was filtered, washed with distilled water, freeze-dried under vacuum overnight, and finally calcined in air at 300 °C for 4 h. The actual Au loading was 0.3–0.4 wt % after DP. The actual Au loading on reference catalysts, Au/Ti–MCM-41 and Au/Ti–MCM-48, respectively, was 0.36 and 0.32 wt %.

2.3. Silylation. Trimethylsilylation of gold–titanosilicate catalysts was carried out by passing methoxytrimethylsilane vapors in Ar stream (at 25 °C) on the catalyst bed for 15–30 min, followed by flushing with Ar at 200 °C (5 h) before catalytic measurements,¹⁶ in order to silylate the titanosilicate support by modifying the silanol (Si–OH) sites with trimethylsilyl (Si–(CH₃)₃) moieties.

2.4. Characterization. The powder X-ray diffraction (XRD) patterns were obtained on a Rigaku Rint-400 instrument equipped with a rotating anode and using Cu Kα radiation (wavelength = 0.1542 nm). UV–vis diffuse reflectance spectra were measured at room temperature on a Photal Otsuka Electronics, MC-2530 instrument. Nitrogen adsorption/desorption isotherms were obtained at –196 °C on a Micromeritics ASAP 2010 apparatus. Prior to measurement, the samples were

heated at 200 °C for 2 h and finally outgassed to 10⁻³ Torr. BET and BJH analysis were used to determine the total specific surface area (*S*_{BET}), pore volume, and pore size distribution of the titanosilicate supports.

X-ray photoelectron spectra were obtained on a Shimadzu ESCA-KM spectrometer equipped with a Mg Kα X-ray exciting source with 10 mA current, 10 kV voltage, and 80 eV pass energy. The O 1s, Si 2p, and Ti 2p core-level spectra were recorded. The binding energies (BE) were referenced to the C 1s peak at 285.0 eV.

The X-ray absorption spectra were collected under ambient conditions on a Rigaku R-EXAFS Super with a rotating W anode X-ray generator operating at 10 kV and 200 mA. The spectral data were collected in transmission mode with 240 s accumulation time. The analysis of the EXAFS data was performed using the Rigaku-EXAFS software to obtain the Ti–O distance of the samples.

Scanning electron microscopy (SEM) observations were made using the Leica Stereoscan 440 model. Transmission electron microscopy (TEM) observations were made using a Hitachi H-9000 instrument to determine the mesoporous structure and Au particle size and its distribution. Actual Au and Ti contents in the catalysts were determined by inductively coupled plasma (ICP) technique.

2.5. Catalytic Activity Measurements. The catalytic tests were carried out in a vertical fixed-bed U-shaped quartz reactor (i.d. 10 mm) at 150–160 °C using a feed containing 10 vol % each C₃H₆, H₂, and O₂ diluted with Ar passed over the catalyst (0.15 g) bed at a space velocity of 4000 h⁻¹ cm³/(g of catalyst). The temperature was measured using a glass tube covered Cr–Al thermocouple located in the center of the catalyst bed. Prior to testing, the catalysts were first pretreated at 250 °C for 30 min. in a stream of 10 vol % H₂ in Ar, followed by 10 vol % O₂ in Ar streams. The feeds and products are analyzed using on-line GCs equipped with TCD (Porapak Q column) and FID (HR-20M column) detectors and autoinjector. Catalysts regeneration was done by treatment in 10 vol % H₂ and O₂ diluted in argon at 250 °C.

3. Results and Discussions

3.1. Powder XRD Analysis. The XRD pattern of mesoporous titanosilicate materials shows a very broad peak around $2\theta = 1.0\text{--}2.0^\circ$ typical for mesostructured materials with a *d*₁₀₀ value of ca. 9.6 nm (Figure 1), which agreed with the distance between the mesopores observed in the TEM image (see inset). Higher order Bragg reflections are not observed for all these samples, indicating the absence of ordered structure in these materials. This observation was also consistent with the high-resolution transmission electron micrograph (HRTEM) image observation, indicating that these samples have a disordered mesostructure with wormhole-like 3D mesoporosity homogeneously distributed throughout the framework structure. Such XRD patterns are similar to those observed for 3D mesostructured materials such as TUD-1,³⁷ HMS,³⁸ MSU-1,³⁶ and KIT-1.³⁹ Visualization of the mesopore connectivity by HRTEM using Pt wires as a contrast agent has shown the presence of 3D connectivity in these materials.³⁷ Also, it was possible to prepare an inverse structure of such materials out of carbon with similar wormhole-like mesoporous structure,³⁷ which supports the presence of a three-dimensional porous network in these materials. In the case of the Ti–Si mixed oxides⁴⁰ prepared by sol–gel procedure⁴¹ without any templating agents, low-angle diffraction peaks have not been observed, indicating the absence of any structural mesoporosity in the framework unit of these mixed oxides.

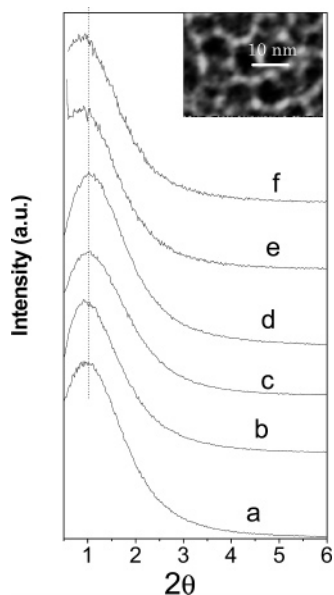


Figure 1. XRD spectra of 3D mesoporous titanosilicates with titanium concentrations of (a) 1.0, (b) 2.0, (c) 3.0, (d) 6.0, (e) 8.0, and (f) 12.0 mol %.

TABLE 1: Porous Properties of Titanosilicate Materials

material(x) ^a	Ti (mol %)	surface area ^c (m ² g ⁻¹)	pore vol ^c (cm ³ g ⁻¹)	pore radius (nm)
meso-Ti-Si(1)	1.0	834	1.1	4.53
meso-Ti-Si(2)	2.0	873	1.4	4.34
meso-Ti-Si(3)	3.0	855	1.2	4.55
meso-Ti-Si(6)	6.0	812	1.1	3.69
meso-Ti-Si(8)	8.0	796	1.1	3.70
meso-Ti-Si(12)	12.0	781	1.0	3.67

^a *x* is the Ti content in mole percent.

High-angle XRD analysis in the 2θ range $20\text{--}30^\circ$ did not show any peaks. The absence of diffraction peak in the 2θ range of $20\text{--}30^\circ$, which is generally attributed to crystalline anatase phase, indicates the existence of well-dispersed titanium in the silica framework with no XRD observable Ti aggregation.

3.2. Nitrogen Adsorption–Desorption Analysis. The BET surface areas of disordered mesoporous materials are found to be lower than those of the ordered MCM-41 type materials (Table 1). Also BJH average pore diameter of these materials is about 7–9 nm, which is much larger than that for MCM type materials (Table 1). All the samples exhibit isotherms of type IV, typical of mesoporous materials, with a well-defined H2 hysteresis loop due to capillary condensation in the mesopores (Figure 2). In general, for all samples the hysteresis loop can be found at the relative pressure of 0.4–0.75. A plateau at the relative pressure of about 0.7 and 1.0 indicates no textural mesoporosity. All the samples exhibit a narrow pore size distribution (Figure 2). Sorption analysis shows that there is little change in the surface properties with increasing Ti concentration in the samples, implying that Ti atoms are either well-dispersed on the walls of the silica matrix or are present inside the framework with no pore blocking effect. After Au deposition the samples show very slight decrease in surface area and pore volume.

3.3. UV–Vis Analysis. The incorporation of Ti into the silica matrix was verified by UV–vis spectral analysis. UV–vis spectra of the titanium-containing mesoporous titanosilicate samples are shown in Figure 3. The UV–Vis analysis of these samples shows a band near the 220 nm range due to tetrahedrally

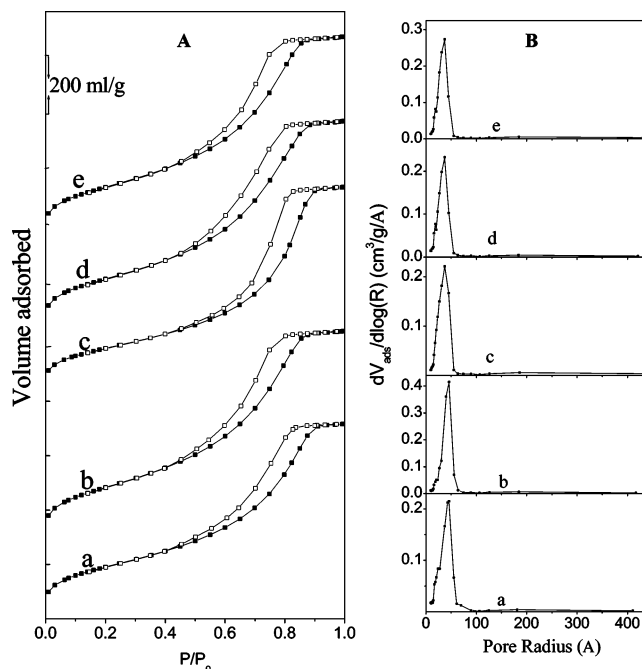


Figure 2. Adsorption isotherm and pore size distribution for 3D mesoporous titanosilicates with titanium concentrations of (a) 2.0, (b) 3.0, (c) 6.0, (d) 8.0, and (e) 12.0 mol %.

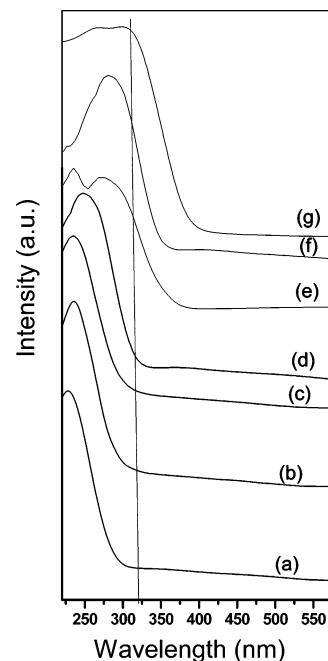


Figure 3. Diffuse reflectance UV–vis spectra of 3D mesoporous titanosilicates with titanium concentrations of (a) 1.0, (b) 2.0, (c) 3.0, (d) 6.0, (e) 8.0, and (f) 12.0 mol % and (g) anatase.

coordinated Ti at lower Ti concentration, which is similar to that for Ti–MCM-41 and Ti–MCM-48 with the same level of Ti content. But with increasing Ti content in the samples the UV–vis spectra were found to become broader at higher wavelength region. The sample with 6 mol % Ti shows a broad band in the region of 220–260 nm. The absorption band at 260–270 nm has been attributed by several researchers to the presence of Ti atoms in 5- and 6-fold coordinations, which are most likely generated through the hydration of the tetrahedrally coordinated sites.^{41,42} The spectra of samples with 2 and 3 mol % Ti shows that Ti is mostly isomorphously substituted for Si in the SiO_4^{4-} tetrahedral and at such low Ti concentrations

TABLE 2: XPS Si/Ti Ratios and O 1s and Ti 2p Binding Energies^a of Mesoporous Titanosilicate Materials

material(x)	(Si/Ti) _{xps}	(Si/Ti) _{bulk} ^b	O 1s, (eV)	Ti 2p _{3/2} (ΔBE ^c) (eV)
meso-Ti–Si(1)	86.5	96.8		459.7 (1.2)
meso-Ti–Si(2)	41.6	53.2	533.1	459.7 (1.2)
meso-Ti–Si(3)	28.2	36.3	533.1	459.5 (1.0)
meso-Ti–Si(6)	13.4	18.9	533.1	459.5 (1.0)
meso-Ti–Si(8)	9.6	13.1		459.4 (0.9)
meso-Ti–Si(12)	6.3	8.1	533.1, 530.1	459.4 (0.9)
anatase			530.1	458.5

^a Reference to the C 1s peak at 285.0 eV. ^b From ICP analysis. ^c ΔBE (in parentheses) corresponds to the increase of the binding energy (BE) with respect to anatase TiO₂.

virtually no Ti–O–Ti linkages are probably present. On the other hand, in the spectra of samples with 8 and 12 mol % Ti, the broad absorption bands centered at 265–280 nm with no clear band at 220 nm. According to earlier reports, this large shift of UV–vis indicates that the Ti atoms would no longer be completely isolated in the silica matrix but would exist in Ti-rich microdomains with Ti–O–Ti linkages that grow progressively larger with increasing Ti content.⁴² Although these shifts might indicate the existence of a small amount of anatase phase in the silica matrix, the calcined samples with up to 12 mol % Ti do not show the presence of any anatase in their XRD patterns as mentioned earlier. Generally a shoulder at ~330 nm is expected in the spectrum if the sample contains some bulk titania, but such a shoulder could not be observed. Yet the formation of Ti–O–Ti clusters with increasing titanium content cannot be ruled out because the spectra become broader and show a red shift with increasing Ti content.

UV–vis spectra are very sensitive to the hydrated state of the Ti-containing silica samples. The spectra of the titanosilicate samples shown in Figure 3 may be different from those measured in the dry state which would result in a large blue shift; for example, mixed oxides with up to 11 mol % Ti after dehydration in a vacuum at 250 °C show a large blue shift of about 30 nm compared to that in the hydrated state.⁴¹ Compared to the UV–vis spectrum of the mixed oxide with 11 mol %, the red shift for the sample with 12 mol % Ti is smaller, indicating that bulk titania phase is absent even at high Ti content and the Ti–O–Ti domains inside these samples are smaller than 1 nm (and so invisible in the XRD spectra).

3.4. XPS Analysis. XPS analysis of titania–silica mixed oxides frequently indicate a linear relationship between surface and bulk composition below about 15 wt % TiO₂, and some surface enrichment in Si, particularly at high Ti content.⁴³ The surface Si enrichment is attributed to the different reactivities of Ti–alkoxide and Si precursors in hydrolysis and condensation reactions during the sol–gel synthesis. The higher reactivity of Ti precursor would lead to the formation of Ti-rich cores in the early stage of synthesis and subsequent development of a Si-rich “shell”. But this effect is minimized in our material, due to Ti–TEA complexation during synthesis, which results in slow and gradual decomposition of this complex leading to incorporation of Ti in the silica matrix, resulting in preferential location of Ti species on the surface. In fact our results shown in Table 2 clearly show the presence of higher surface Ti content, which can be attributed to the role of TEA which slows down the hydrolysis of Ti precursor. Higher surface Ti content would result in a greater number of exposed active surface Ti sites that would lead to better catalytic performance which was found to be true (vide infra).

The binding energies (BE) of Ti 2p_{3/2} and O 1s core level of 3D mesoporous titanosilicate samples are collected in Table 2,

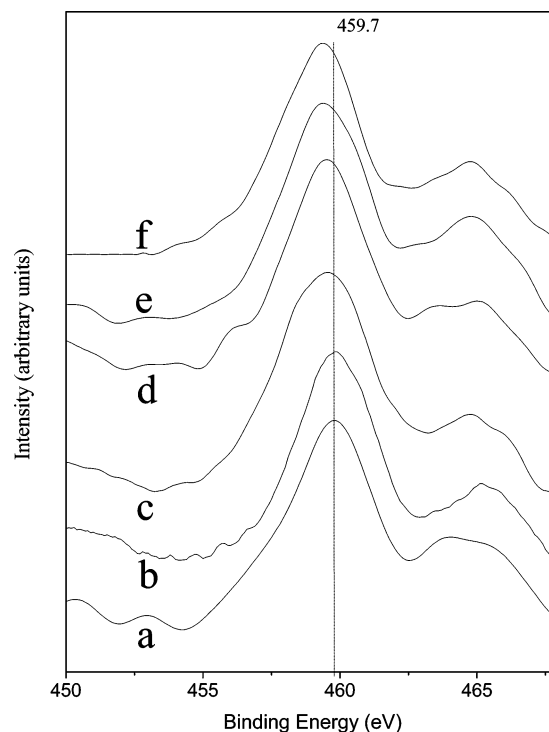


Figure 4. Ti 2p XPS spectra of 3D mesoporous titanosilicates with titanium concentrations of (a) 1.0, (b) 2.0, (c) 3.0, (d) 6.0, (e) 8.0, and (f) 12.0 mol %.

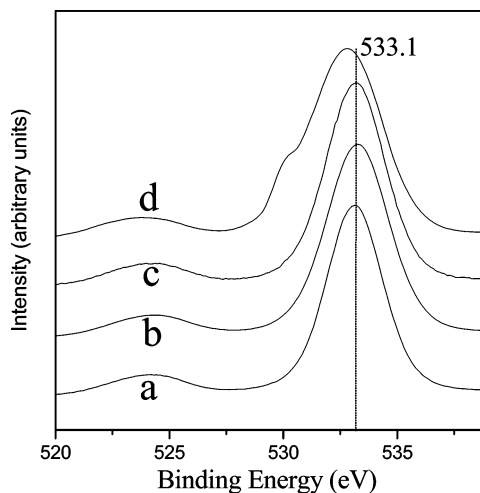


Figure 5. O 1s XPS spectra of 3D mesoporous titanosilicates with titanium concentrations of (a) 2.0, (b) 3.0, (c) 6.0, and (d) 12.0 mol %.

and the corresponding spectra are shown in Figures 4 and 5. Figure 4 shows Ti 2p XPS spectra as a Ti 2p_{3/2} and Ti 2p_{1/2} doublet with a separation of 5.75 eV for the samples with different titanium content. With low titanium content, samples show a Ti 2p_{3/2} line at 459.7 eV binding energy, which is about 1 eV higher than that of TiO₂ anatase⁴⁴ and indicates tetrahedral coordination of completely isolated Ti sites in the silica matrix.⁴⁵ With increasing titanium loadings the positions of the Ti 2p line shift toward lower binding energies. As the titanium loading increases for Ti > 6 mol %, the Ti 2p_{3/2} line shifts further toward the binding energy of Ti 2p_{3/2} measured for TiO₂ anatase (458.5 eV),⁴⁴ but still a gap of approximately 0.9 eV is obvious. Lassaletta et al.⁴⁶ proposed that, in addition to the effect of coordination environment, the titania–silica interface is important for the BE in XPS measurements. At the Ti–O–Si interface, the oxygen is less polarizable than bulk titania and the photoelectrons created at the titania–silica interface are less

efficiently screened than bulk titania. Thus, the shift in the position of the Ti 2p line toward lower binding energies with increasing Ti loading reveal an incomplete Ti site isolation and the presence of Ti-rich microdomains with Ti–O–Ti linkages at high Ti content.

Figure 5 shows O 1s XPS spectra of titanosilicates with different titanium loadings. Only an intense O 1s line at 533.1 eV is observed for samples up to 6 mol % Ti. For highest titanium loading of 12 mol %, a weak O 1s line at 530.2 eV becomes resolvable, indicating the presence of TiO₂ clusters. TiO₂ anatase gives only one line at 530.2 eV.

3.5. XANES Analysis. XANES represents electronic transition from an inner level to the outer unoccupied levels caused by X-ray absorption, thus giving information on the local electronic structure and coordination environment around an absorbing atom. For this reason, the coordination state of Ti has often been probed by Ti K-edge XANES in a qualitative manner by comparison of shape or intensity of preedge peak with XANES spectra of reference materials. The characteristic feature in Ti K-edge spectra is the preedge caused by the excitation of 1s electron into an empty bound state derived from d and p states of Ti and O. It is well-known that Ti(IV) is in a d⁰ configuration corresponding to A₁ or A_{1g} states depending on tetrahedral or octahedral symmetry with four or six oxygen anions, respectively.⁴⁷ In the tetrahedral symmetry, transitions occur from A₁ into the final states of T₂ and E. As considerable mixing of 3d and 4p orbitals occurs, the A₁-into-T₂ transition is allowed and overwhelms the weaker A₁-into-E transition. Therefore, tetrahedral Ti(IV) is represented by a strong single peak in the preedge region. In the case of octahedral symmetry, the transition of 1s electrons occurs into empty d orbitals and the final states are T_{2g} and E_g. Hence, expected transitions are A_{1g}-into-T_{2g} and E_g, which are both Laporte-forbidden. Consequently, the octahedral symmetry of Ti(IV) shows weaker preedge absorption peaks than that for tetrahedral Ti(IV).^{41,42,47} We investigated the Ti K-edge XANES spectra of the samples with different Ti concentrations as presented in Figure 6. Attention was focused on the change in preedge peak intensity as the amount of Ti was increased. Compared with the preedge peak for the 6 mol % Ti sample (Figure 6b), the intensities for the 3 mol % Ti sample (Figure 6a) was smaller. It is evident that the formation of the Ti–O–Si connectivity having tetrahedral symmetry of Ti with four surrounding O anions was maximized at Ti = 6 mol %. For the samples with 12 mol % Ti (Figure 6c), the intensity of the main preedge peak decreased and a weak shoulder peak (indicated by arrow) appeared next to the main preedge peak, which could be interpreted as the preedge peak of anatase. It implies formation of some Ti–O–Ti bonds having octahedral symmetry of Ti, but no titania phase was detected by XRD analysis indicating the presence of well-dispersed and very small Ti–O–Ti clusters. It is well-known that water adsorption disturbs the regular tetrahedral symmetry of Ti in a silica-rich sample, and the XANES spectra are very sensitive to the hydrated state of Ti. So the presence of five- and six-coordinated Ti sites generated through the hydration of tetrahedral sites cannot be ruled out.^{41,42,47}

EXAFS region of the absorption spectra provided complementary information on the local environment surrounding Ti. A Fourier transform of the EXAFS data in Figure 6 provided the Ti–O distance of 0.181 nm for the sample with 6 mol % Ti, while it was slightly higher at 0.188 for the 12 mol % Ti sample. The average Ti–O distance in 4-fold and 6-fold coordinated silicates has been reported to be 0.179–0.184 and 0.194–0.206 nm, respectively.⁴⁸

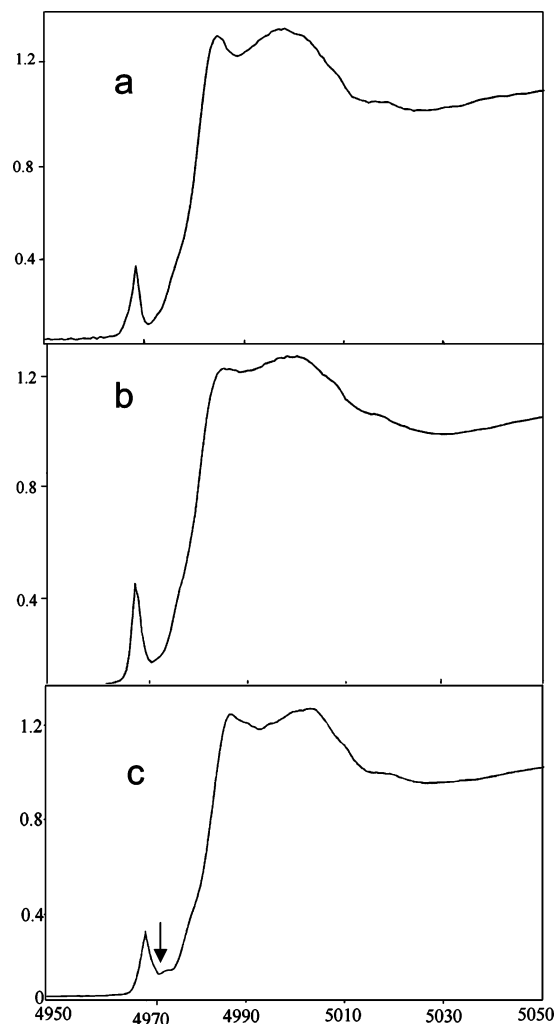


Figure 6. Ti K-edge X-ray absorption spectra of 3D mesoporous titanosilicates with titanium concentration of (a) 3.0, (b) 6.0, and (c) 12.0 mol %.

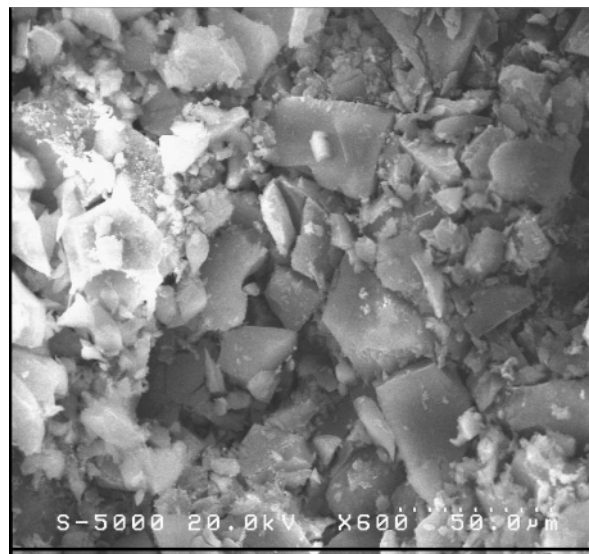


Figure 7. SEM of 3D mesoporous titanosilicate support with 2.0 mol % Ti content.

3.6. SEM and TEM Analysis. SEM analysis of these samples (Figure 7) showed that the particles did not have any well-defined morphology and the sample consisted of about 5–50 μ m irregular-shaped cheeselike particles. TEM analysis clearly shows (Figure 8) that the mesoporous network is

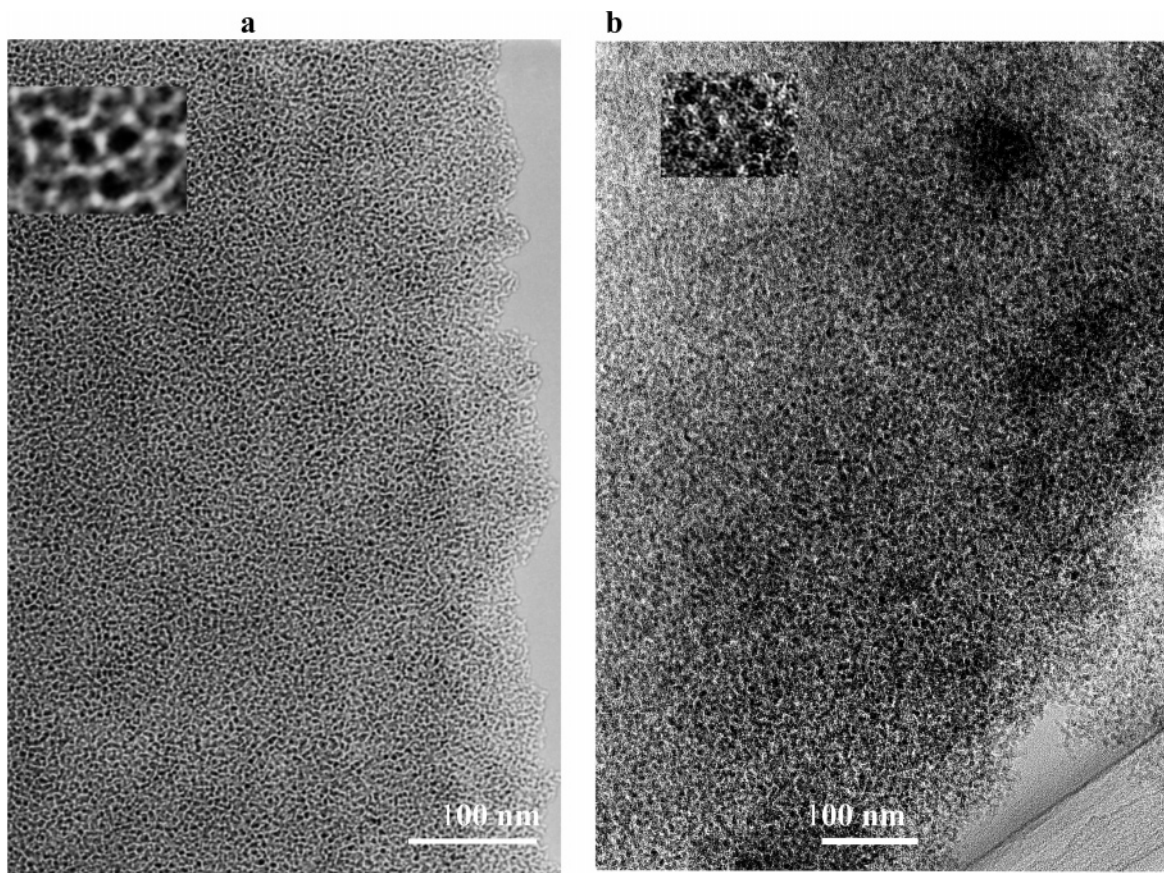


Figure 8. TEM of 3D mesoporous titanosilicate supports with (a) 2 and (b) 12 mol % Ti.

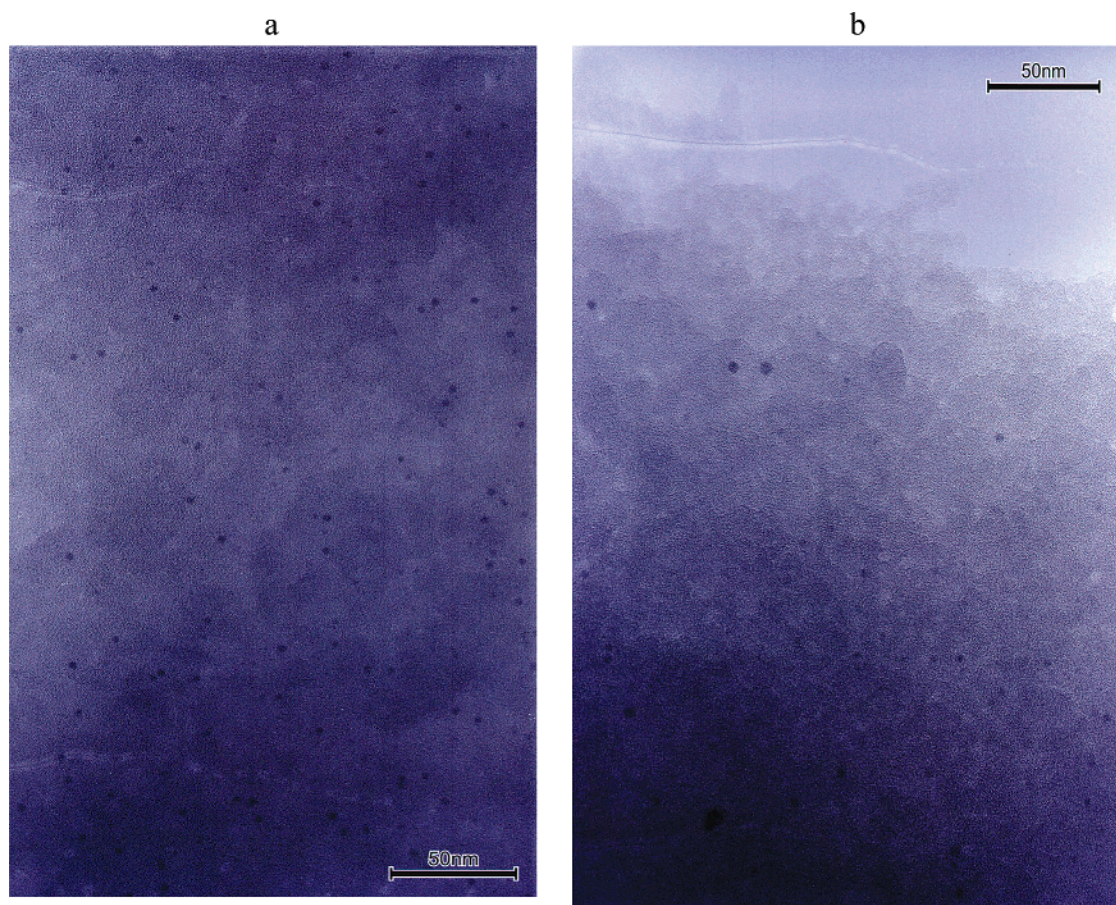


Figure 9. TEM of 4% Au deposited titanosilicate supports with (a) 2.0 and (b) 6.0 mol % Ti.

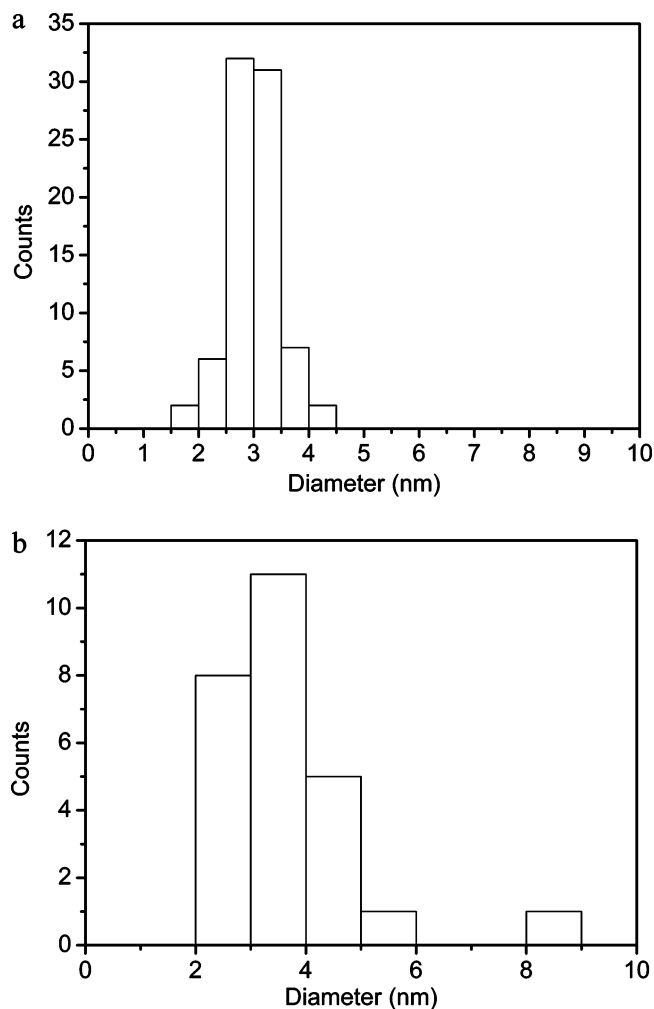


Figure 10. Particle size distribution for 4% Au deposited titanosilicate supports with (a) 2.0 and (b) 6.0 mol % Ti.

homogeneously distributed throughout the framework structure. The Figure 8 inset clearly shows the presence of well-defined mesopores in these samples. TEM of the sample with 12 mol % Ti shows a rather foamlike mesoporous structure.

3.7. Gold Nanoparticles Distribution on Supports. TEM analysis of the supported gold catalysts (Figure 9) clearly shows the presence of homogeneously distributed Au nanoparticles on the support surface. The samples show a narrow gold particle size distribution (Figure 10) with average particles size of about 3.0 ± 1 nm. The supports with higher Ti content (6 mol %) show the presence of some larger Au nanoparticles (Figure 9b). The reference catalysts, Au/Ti-MCM-41 and Au/Ti-MCM-48 also had average particle size of 3.0 ± 1 nm.

We have observed that sequential pretreatments, using diluted H_2 followed by diluted O_2 , is very vital for obtaining highly dispersed nano-Au catalysts with narrow particle size distribution in the range of 2–5 nm, which results in high catalytic activity. Only H_2 pretreatment resulted in smaller Au particles, with considerable number of particles with <2 nm size, which results in significant decrease in epoxidation activity (about 10–15% lower activity). It is likely that O_2 induces the growth of Au particles because the pretreatment only in the diluted H_2 did not cause appreciable growth of Au particles.¹⁶

3.8. Propylene Epoxidation Activity. (a) *Support Effect.* Figure 11 shows the results of propylene epoxidation over Au-deposited, 3D mesoporous titanosilicates (meso-Ti-Si), silylated meso-Ti-Si, and mesoporous Ti-MCM-41 and Ti-MCM-48. It is observed that meso-Ti-Si samples are more active as

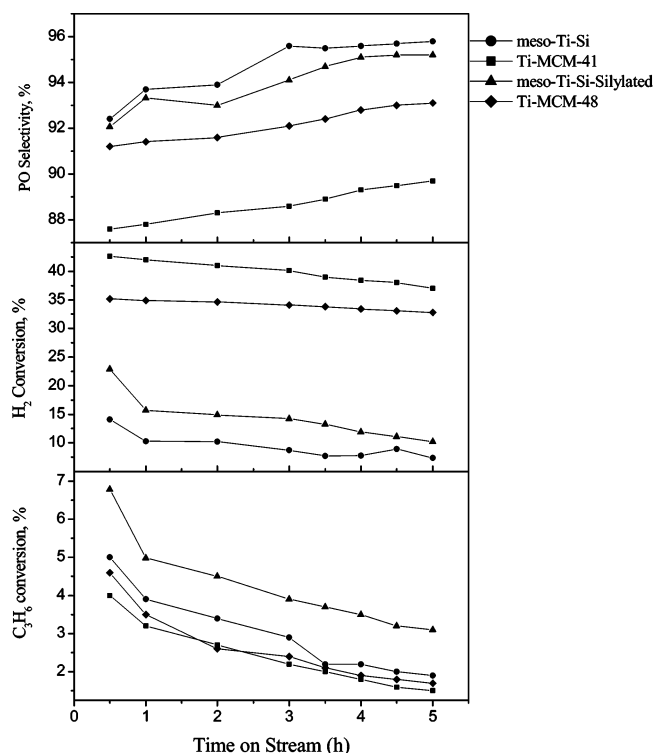


Figure 11. Propylene conversion, PO selectivity, H_2 conversion, and PO yield on various mesoporous titanosilicate supported Au catalysts.

supports for nanogold catalysts and exhibit higher propene conversion and PO selectivity than Ti-MCM-41 and Ti-MCM-48. Enhanced propene conversion and PO selectivity can be attributed to larger pore size and 3D mesoporosity of the support for easy diffusion of reactants and products as well as due to higher concentration of surface Ti sites (as observed by XPS analysis). Propene conversion is further enhanced after silylation of the gold-titanosilicate catalysts. Such an enhancement in conversion after silylation was not observed in the case of ordered Ti-MCM-48 based catalyst.^{16,25} Also, these titanosilicate-based catalysts showed the best hydrogen efficiency. For example, the H_2 consumption was nearly 2–5 times less than those observed for the ordered MCM-41 and MCM-48 type supports, which can be directly correlated to efficient utilization of in situ generated hydrogen peroxide-like species for epoxidation³ due to better synergism between Au and Ti sites.

(b) *Ti Concentration Effect.* Figure 12 shows the influence of variation in Ti content from 2 to 6 mol % in the gold-titanosilicate catalysts on propylene epoxidation performance. The propylene conversion increased slightly while the PO selectivity decreased, with the increasing Ti content. PO yield is found to increase with increasing Ti content, the catalyst with 6 mol % Ti content gives the highest PO yield while the catalyst with 2 mol % Ti content gives the lowest PO yield. The catalyst with 2 mol % Ti content showed the best hydrogen efficiency. But in the case of MCM-41 and MCM-48 supported Au catalysts the best catalyst performance was obtained with only 1.5–2 mol % Ti concentration when the Ti isolation in silica matrix was optimum.^{14–16} Better Ti dispersion in silica matrix for the 3D wormhole-like mesoporous titanosilicate even at higher Ti contents (up to 6 mol %) (as observed by UV-vis analysis) and a greater amount of surface-exposed Ti sites (as observed by XPS analysis) could be responsible for better catalytic performance of the catalysts.

(c) *Trimethylsilylation Effect.* Figures 13 and 14 show the results of the influence of trimethylsilylation of 3D mesoporous

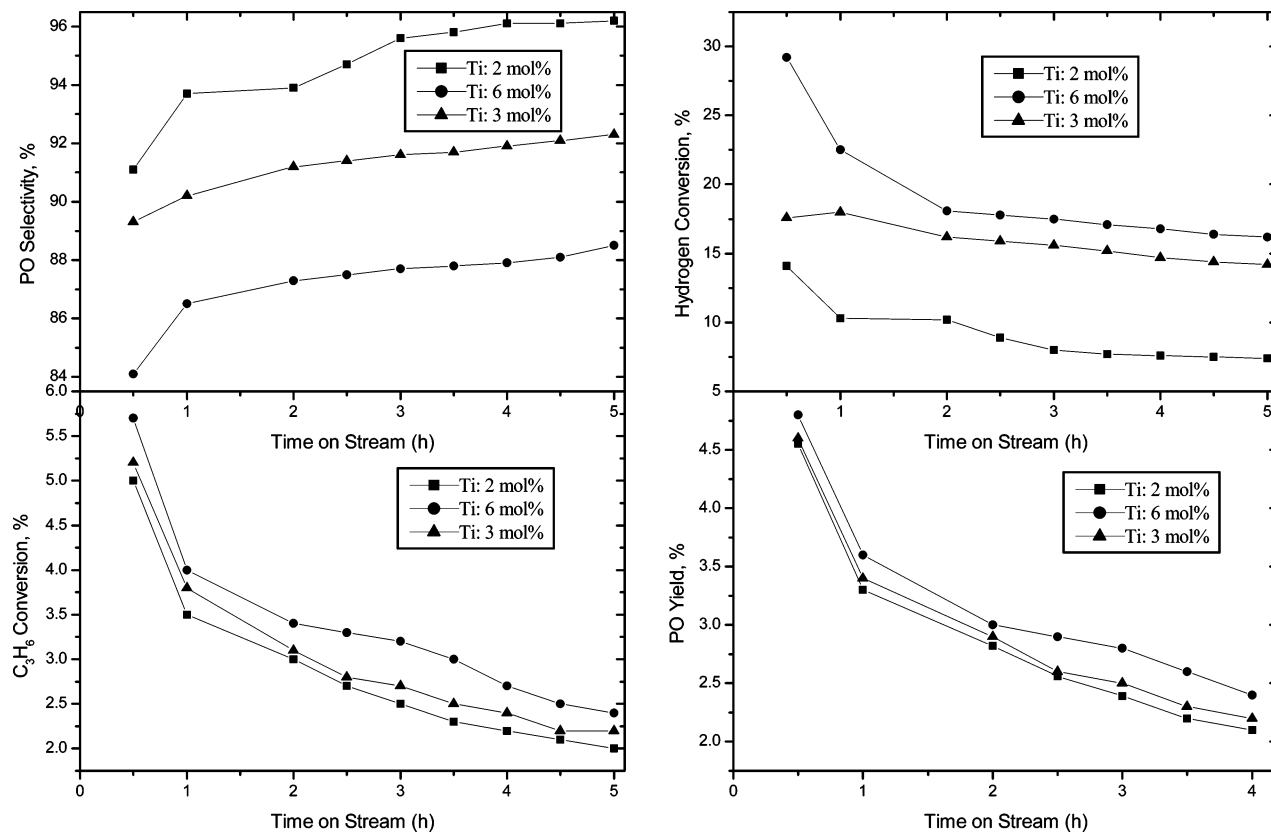


Figure 12. Propylene conversion, PO selectivity, H₂ conversion, and PO yield on mesoporous titanasilicate supported Au catalysts with different Ti concentrations.

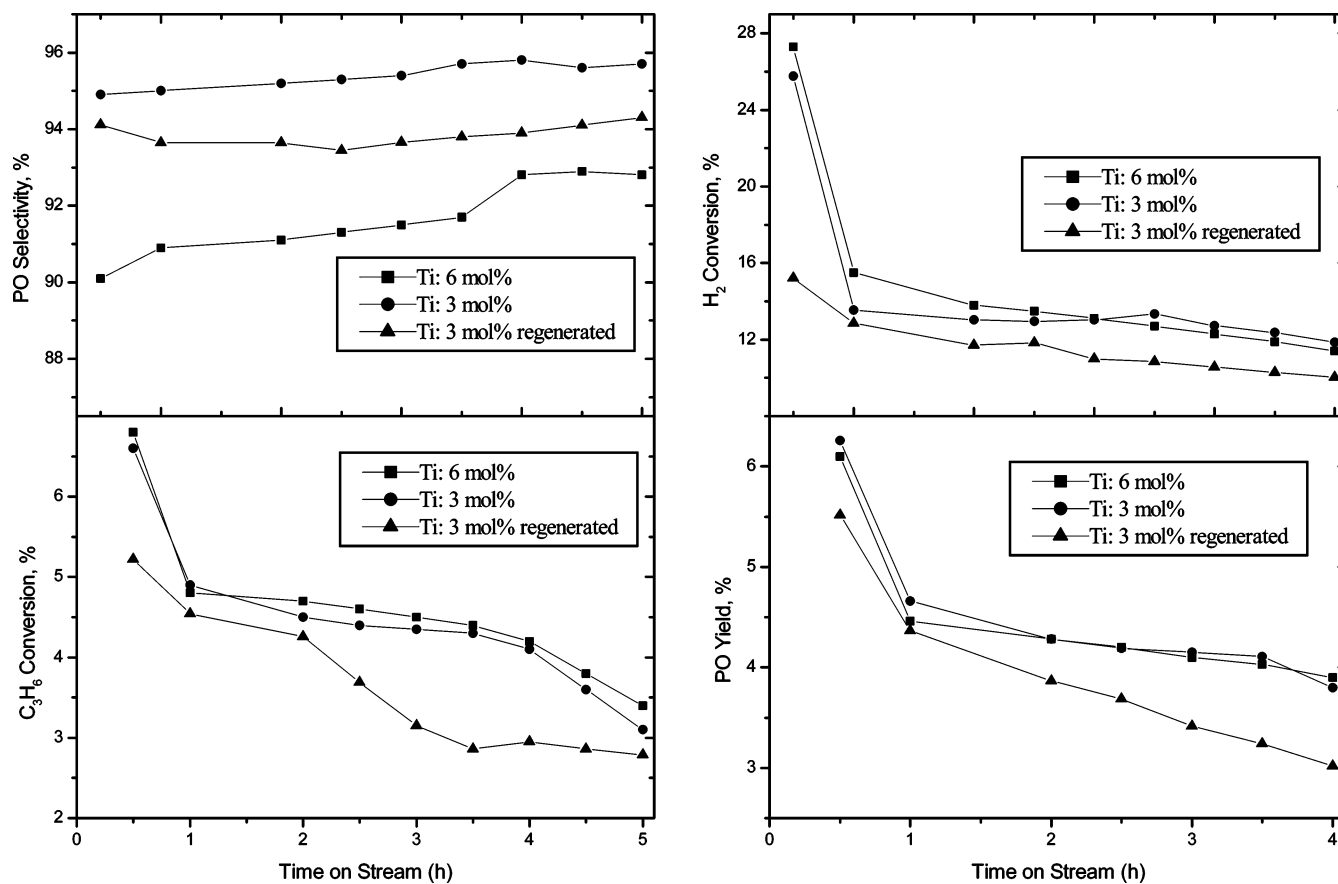


Figure 13. Propylene conversion, PO selectivity, H₂ conversion, and PO yield on mesoporous titanasilicate supported Au catalysts with 3.0 and 6.0 mol % Ti concentrations after trimethylsilylation and after regeneration of silylated 3.0 mol % Ti catalyst.

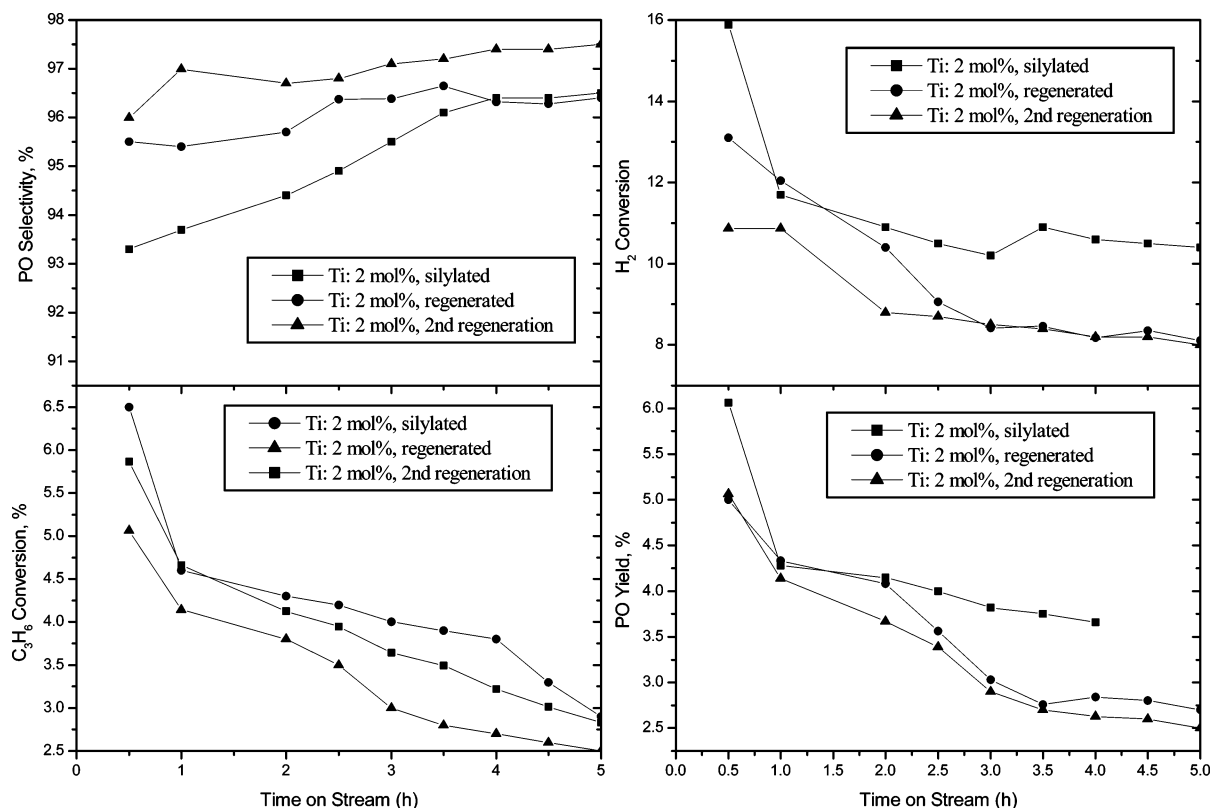


Figure 14. Propylene conversion, PO selectivity, H₂ conversion, and PO yield on silylated mesoporous titanosilicate supported Au catalyst with 2.0 mol % Ti, before and after regeneration.

gold–titanosilicate catalysts with different Ti concentrations on propene epoxidation performance. Under similar reaction conditions, the silylated catalysts showed much enhanced activity for propene epoxidation compared to the unsilylated catalyst (see Figure 12). The propene conversion as well as PO selectivity increased conspicuously after silylation of gold–titanosilicate catalysts. There was more than 40% increase in PO yield after silylation. The silylated catalysts with 3 and 6% Ti concentrations showed higher propene conversion as well as PO yield compared to 2% Ti content silylated catalyst. Higher hydrophobicity for the silylated catalysts, due to formation of trimethylsilyl moiety after silylation of the silanol sites of titanosilicate support, favors easy desorption of PO from the catalyst, thereby showing marked improvement in PO yield for these catalysts. Propene conversions decreased with reaction time on stream for all the catalysts, but a relatively lower decrease was observed in the case of silylated catalysts. This is attributable to the easy desorption of PO from the support surface as well as due to passivation of surface acid sites, thereby preventing the deactivation of the catalyst surface by oligomerized species formed from the adsorbed PO at the acid sites.¹⁶ Thus, silylation of Au catalysts supported on disordered titanosilicates has been found to have a very positive influence on PO yield in contrast to the case of silylated Au/Ti–MCM-48 catalysts.¹⁶ It is interesting to note from Figure 13 that the silylated catalysts with 3 and 6 mol % Ti content show marked decrease in H₂ conversion compared to the unsilylated catalysts (see Figure 12).

(d) *Catalysts Regeneration.* Fast deactivation of the catalyst is a major problem in this reaction. IR spectroscopic studies²⁴ have identified propoxy groups formed from the adsorbed PO, which might form oligomerized species responsible for deactivation. Attempts to regenerate the deactivated catalysts by thermal treatment in oxygen stream, or by dissolving in organic

solvents the deactivating organic moieties from the catalyst surface, failed to recover the original activity of the catalyst. But, we could demonstrate for the first time that it was possible to regenerate the catalysts to regain more than 80% of the initial activity by treatment in 10 vol % H₂ and O₂ diluted in argon (for about 1–2 h) at 250 °C. Figures 14 and 13 compare the performance of the regenerated silylated catalysts after 48 h of reaction. The catalyst after regeneration showed improved PO selectivity and hydrogen efficiency. The local heat generated during the reaction of H₂ and O₂ at the active sites of the catalyst during regeneration is probably responsible for the elimination of the accumulated deactivating species at the active sites. The regenerated catalysts maintained their XRD crystallinity, and there was little decrease in the surface areas compared to the fresh catalyst. Also, UV–vis analysis did not show any change in the band near 220 nm observed for the fresh sample, indicating that the regenerated samples maintain the tetrahedral coordination of Ti species.

The catalysts are found to be very active and selective even on regenerating after two reaction cycles (Figure 14). The reaction over the second regeneration catalyst was performed at 160 °C, while for all other catalysts the reaction temperature was 150 °C. The reason for selecting higher reaction temperature for the second regeneration catalyst was that it was possible to have high conversions with optimum PO selectivity and hydrogen efficiencies, whereas in the case of fresh as well as first regeneration catalysts, the best hydrogen efficiency and PO yield were obtained at 150 °C (Figure 14). The possibility of regenerating the used catalysts is very important in order to make this process commercially viable.

4. Conclusions

We could prepare high surface area, high Ti content 3D wormhole-like mesoporous materials with high Ti dispersion

in silica matrix as observed by physicochemical and spectroscopic characterizations. These mesoporous titanosilicates with wormhole-like 3D mesoporosity and with Ti content as high as 6 mol % are found to be highly efficient catalysts for vapor-phase propylene epoxidation using O₂ and H₂, after Au deposition followed by trimethylsilylation. About 7% propylene conversion at >90% PO selectivity and about 40% hydrogen efficiency could be achieved using these catalysts. Three-dimensional mesoporosity, large mesopores (>7 nm pore size) allowing better dispersion of Au nanoparticles inside the mesopores, and enhanced hydrophobicity due to silylation were responsible for achieving close to commercially desired propene epoxidation performance.

These 3D mesoporous titanosilicates with wide composition range, high specific surface area, and high degree of homogeneous Ti dispersion can have potential application as catalyst and support for a variety of reactions, as well as find application in adsorption, coatings, and membranes.

References and Notes

- (1) Ainsworth, S. J. *Chem. Eng. News* **1992**, 9. McCoy, M. *Chem. Eng. News* **2001**, 79, 19.
- (2) Clerici, M. G.; Bellusi, G.; Romano, U. *J. Catal.* **1991**, 129, 159.
- (3) Notari, B. *Catal. Today* **1993**, 18, 163.
- (4) Occhiello, E. *Chem. Ind.* **1997**, 761.
- (5) Sato, A.; Miyake, T.; Saito, T. *Shokubai (Catalysts)* **1992**, 34, 132.
- (6) Meiers, R.; Dingerdisen, U.; Hölderich, W. F. *J. Catal.* **1998**, 176, 376.
- (7) Hayashi, T.; Tanaka, K.; Haruta, M. *J. Catal.* **1998**, 178, 566.
- (8) Haruta, M. *Catal. Surv. Jpn.* **1997**, 1, 61, and references therein.
- (9) Haruta, M. *Catal. Today* **1997**, 36, 123, and references therein.
- (10) Hayashi, T.; Tanaka, K.; Haruta, M. *Shokubai* **1995**, 37, 72.
- (11) Kalvachev, Y. A.; Hayashi, T.; Tanaka, K.; Haruta, M. *Stud. Surf. Sci. Catal.* **1997**, 110, 965.
- (12) Haruta, M.; Uphade, B. S.; Tsubota, S.; Miyamoto, A. *Res. Chem. Intermed.* **1998**, 24, 329.
- (13) Qi, C.; Okumura, M.; Akita, T.; Haruta, M. *Appl. Catal., A* **2004**, 263, 19.
- (14) Uphade, B. S.; Okumura, M.; Tsubota, S.; Haruta, M. *Appl. Catal., A* **2000**, 190, 43.
- (15) Uphade, B. S.; Yamada, Y.; Akita, T.; Nakamura, T.; Haruta, M. *Appl. Catal., A* **2001**, 215, 137.
- (16) Uphade, B. S.; Akita, T.; Nakamura, T.; Haruta, M. *J. Catal.* **2002**, 209, 331.
- (17) Sinha, A. K.; Seelan, S.; Akita, T.; Tsubota, S.; Haruta, M. *Appl. Catal., A* **2003**, 240, 243.
- (18) Sinha, A. K.; Akita, T.; Tsubota, S.; Haruta, M. *Stud. Surf. Sci. Catal.* **2002**, 142, 611.
- (19) Sinha, A. K.; Seelan, S.; Tsubota, S.; Haruta, M. *Stud. Surf. Sci. Catal.* **2002**, 143, 167.
- (20) Sinha, A. K.; Seelan, S.; Akita, T.; Tsubota, S.; Haruta, M. *Catal. Lett.* **2003**, 85, 223.
- (21) Kapoor, M. P.; Sinha, A. K.; Seelan, S.; Inagaki, S.; Tsubota, S.; Yoshida, H.; Haruta, M. *Chem. Commun.* **2002**, 2902.
- (22) Nijhuis, T. A.; Huizinga, H.; Makkee, M.; Moulijn, J. A. *Ind. Eng. Chem. Res.* **1999**, 38, 884.
- (23) Stangland, E. E.; Stavens, K. B.; Andres, R. P.; Delgass, W. N. *J. Catal.* **2000**, 191, 332.
- (24) Mul, G.; Zwijnenburg, A.; Linden, B.; van der Makkee, M.; Moulijn, J. A. *J. Catal.* **2001**, 201, 128.
- (25) Sinha, A. K.; Seelan, S.; Tsubota, S.; Haruta, M. *Angew. Chem., Int. Ed.* **2004**, 43, 1546.
- (26) Kresge, C. T.; Leonowicz, M. E.; Roth, W. J.; Vartuli, J. C.; Beck, J. S. *Nature* **1992**, 359, 710.
- (27) Corma, A. *Chem. Rev.* **1997**, 97, 2373.
- (28) Notari, B. *Adv. Catal.* **1996**, 41, 253.
- (29) Zhang, W.; Froba, M.; Wang, J.; Tanev, P. T.; Wong, J.; Pinnavaia, T. J. *J. Am. Chem. Soc.* **1996**, 118, 9164.
- (30) Maschmeyer, T.; Rey, F.; Sankar, G.; Thomas, J. M. *Nature* **1995**, 378, 159.
- (31) Dusi, M.; Mallat, T.; Baiker, A. *Catal. Rev. – Sc. Eng.* **2000**, 42, 213.
- (32) Tanev, P. T.; Chibwe, M.; Pinnavaia, T. J. *Nature* **1994**, 368, 321.
- (33) Bhaumik, A.; Tatsumi, T. *J. Catal.* **2000**, 189, 31.
- (34) Corma, A.; Garcia, H.; Navarro, M. T.; Palomares, E. J.; Rey, F. *Chem. Mater.* **2000**, 12, 3068.
- (35) Sever, R. R.; Root, T. W. *J. Phys. Chem. B* **2003**, 107, 4080.
- (36) Bagshaw, S. A.; Prouzet, E.; Pinnavaia, T. J. *Science* **1995**, 269, 1242.
- (37) Jansen, J. C.; Shan, Z.; Marchese, L.; Zhou, W.; Puil, N. v. d.; Maschmeyer, T. *Chem. Commun.* **2001**, 713. Shan, Z.; Gianotti, E.; Jansen, J. C.; Peters, J. A.; Marchese, L.; Maschmeyer, T. *Chem. Eur. J.* **2001**, 7, 1437.
- (38) Tanev, P. T.; Pinnavaia, T. J. *Science* **1995**, 267, 865.
- (39) Ryoo, R.; Kim, J. M.; Ko, C. H.; Shin, C. H. *J. Phys. Chem.* **1996**, 100, 17718.
- (40) Soult, A. S.; Carter, D. F.; Schreiber, H. D.; van de Burgt, L. J.; Stiegman, A. E. *J. Phys. Chem. B* **2002**, 106, 9266.
- (41) Davis, R. J.; Liu, Z. *Chem. Mater.* **1997**, 9, 2311.
- (42) Liu, Z.; Crumbaugh, G. M.; Davis, R. J. *J. Catal.* **1996**, 159, 83.
- (43) Gao, X.; Bare, S. R.; Fierro, J. L. G.; Banares, M. A.; Wachs, I. E. *J. Phys. Chem. B* **1998**, 102, 5653.
- (44) Galan-Fereres, M.; Alemany, L. J.; Mariscal, R.; Banares, M. A.; Anderson, J. A.; Fierro, J. L. G. *Chem. Mater.* **1995**, 7, 1342.
- (45) Stakheev, A. Y.; Shpiro, E. S.; Apijok, J. *J. Phys. Chem.* **1993**, 97, 5668.
- (46) Lassaletta, G.; Fernandez, A.; Espinos, J. P.; Gonzalez-Elipe, A. R. *J. Phys. Chem. B* **1995**, 99, 1484.
- (47) Bordiga, S.; Coluccia, S.; Lamberti, C.; Marchese, L.; Zecchina, A.; Boscherini, F.; Buffa, F.; Genoni, F.; Leofanti, G.; Petrini, G.; Vlaic, G. *J. Phys. Chem.* **1994**, 98, 4125.
- (48) Blasco, T.; Corma, A.; Navarro, M. T.; Pariente, J. P. *J. Catal.* **1995**, 156, 65.